Comprehensive analysis of MRI protocol for detection of liver metastases from melanoma

Hyun Jung Chung

The Graduate School
Yonsei University
Department of Medicine

Comprehensive analysis of MRI protocol for detection of liver metastases from melanoma

A Dissertation Submitted
to the Department of Medicine
and the Graduate School of Yonsei University
in partial fulfillment of the
requirements for the degree of
Doctor of Philosophy in Medical Science

Hyun Jung Chung

December 2024

This certifies that the Dissertation of Hyun Jung Chung is approved

Thesis Supervisor Nieun Seo

Thesis Committee Member Yong Eun Chung

Thesis Committee Member Minkyu Jung

Thesis Committee Member Kyunghwa Han

Thesis Committee Member Bo Hyun Kim

The Graduate School
Yonsei University
December 2024

ACKNOWLEDGEMENTS

I wish to extend my profound gratitude to Professor Nieun Seo for her unwavering support and wholehearted dedication throughout the entirety of this research endeavor. Her guidance and encouragement have been invaluable, and I am immensely thankful for her mentorship.

Furthermore, I would like to express my heartfelt appreciation to the esteemed members of the committee for their generous insights and words of encouragement, graciously provided amidst their demanding schedules.

TABLE OF CONTENTS

LIST OF FIGURES ····· iii
LIST OF TABLES ····· iv
ABSTRACT IN ENGLISH ····· V
1. INTRODUCTION ····· 1
2. MATERIALS AND METHODS ····· 2
2.1 Gadoxetic acid-enhanced MRI for detection of liver metastases from melanoma ····· 2
2.1.1 Study population ····· 2
2.1.2 Acquisition of MRI ····· 3
2.1.3 Image analysis ····· 3
2.1.4 Data and statistical analysis ····· 4
2.2 Non-contrast liver MRI as an alternative to gadoxetic acid-enhanced MRI for detection of uveal melanoma liver metastasis ····· 5
2.2.1 Study population ····· 5
2.2.2 Acquisition of MRI ····· 5
2.2.3 Image analysis ····· 5
2.2.4 Data and statistical analysis ····· 6
3. RESULTS ····· 5
3.1 Gadoxetic acid-enhanced MRI for detection of liver metastases from melanoma ····· 6
3.1.1 Patient characteristics ····· 6
3.1.2 Gadoxetic acid-enhanced MRI features of melanoma liver metastases ····· 8
3.1.3 Comparison of detection sensitivity for liver metastasis among different MR sequences ····· 14
3.2 Non-contrast liver MRI as an alternative to gadoxetic acid-enhanced MRI for detection of uveal melanoma liver metastasis ····· 17
3.2.1 Patient characteristics ····· 17
3.2.2 Diagnostic performance of abbreviated MRI sets to detect uveal melanoma liver metastases ····· 18
4. DISCUSSION ····· 21
4.1 Gadoxetic acid-enhanced MRI for detection of liver metastases from melanoma ····· 21
4.2 Non-contrast liver MRI as an alternative to gadoxetic acid-enhanced MRI for detection of uveal melanoma liver metastasis ····· 23
5. CONCLUSION ····· 25

REFERENCES ··· 26
ABSTRACT(IN KOREAN) ·· 29

LIST OF FIGURES

<Fig 1> Patient flow diagram ····· 7
<Fig 2> Gadoxetic acid-enhanced MRI in a 53-year-old woman with liver metastases from uveal (choroidal) melanoma ····· 12
<Fig 3> Gadoxetic acid-enhanced MRI in a 59-year-old man with liver metastases from non-uveal (oral mucosal) melanoma ····· 13
<Fig 4> Patient flow diagram ····· 17
<Fig 5> Gadoxetic acid-enhanced MRI in a 78-year-old woman with liver metastases from uveal (choroidal) melanoma ····· 20

LIST OF TABLES

<Table 1> Patient demographics in first study ····· 8
<Table 2> MR findings of liver metastases according to the detection on the hepatobiliary phase 9
<Table 3> MR findings of liver metastases according to the primary site of melanoma ····· 11
<Table 4> Comparison of detection sensitivity of MR imaging sets according to lesion size and primary site ····· 14
<Table 5> Comparison of detection sensitivity of HBP and each imaging set according to lesion size and primary site ····· 15
<Table 6> Inter-reader agreement of the MRI evaluation ····· 16
<Table 7> Patient demographics in second study ····· 18
<Table 8> Overall diagnostic performance for detection of hepatic metastases ····· 19
<Table 9> Sensitivities for detection of hepatic metastases ····· 19
<Table 10> Positive predictive values for detection of hepatic metastases ····· 21

ABSTRACT

Comprehensive analysis of MRI protocol for detection of liver metastases from melanoma

Objectives:

This study provides a comprehensive analysis of magnetic resonance imaging (MRI) protocols for the detection of liver metastases from melanoma.

Methods:

1. Gadoxetic acid-enhanced MRI for detection of melanoma

This retrospective study included 67 patients with melanoma liver metastasis who underwent gadoxetic acid-enhanced MRI. Two abdominal radiologists independently evaluated signal characteristics of liver metastases on morphologic imaging (precontrast T1- and T2-weighted imaging), diffusion-weighted imaging (DWI), dynamic imaging, and hepatobiliary phase (HBP). Imaging findings were compared according to detection on HBP and the primary site of melanoma. Detection sensitivity for metastases was compared among different MR imaging sets using logistic regression with the generalized estimating equation.

2. Non-contrast liver MRI as an alternative to gadoxetic acid-enhanced MRI for detection of uveal melanoma liver metastasis

This retrospective study included 27 uveal melanoma patients who underwent gadoxetic acid-enhanced MRI for suspected liver metastasis. Two independent readers reviewed three MR imaging sets: NC-MRI (T1-weighted, T2-weighted, and diffusion-weighted imaging), dynamic-MRI (NC-MRI and dynamic phases), and full-MRI (dynamic-MRI and HBP) to detect hepatic metastases. Overall diagnostic performance for detecting metastases was evaluated using alternative free-response receiver operating characteristic curve analysis. The sensitivity, and positive predictive value (PPV) were compared among imaging sets by using logistic regression with generalized estimating equations.

Results:

1. Gadoxetic acid-enhanced MRI for detection of melanoma

A total of 67 patients with 254 liver metastases were included (44 women; mean age ± standard

deviation, 65.6 ± 13.0 years). On HBP, 76.0% (193/254) of metastases were detected, and 55.5% (141/254) showed hypointensity. Most of the metastases that were not detected on HBP originated from uveal melanomas (98.4%, 60/61), ≤1 cm (90.2%, 55/61), and showed T1 hyperintensity (98.4%, 60/61). Metastases from non-uveal melanomas more frequently showed T1 hypointensity, T2 hyperintensity, diffusion restriction, arterial enhancement, and HBP hypointensity than those from uveal melanomas (*P*s ≤ 0.019). The detection sensitivity of HBP (76.0%) was significantly higher than DWI (65.7%, *P* = 0.006), but lower than morphologic imaging (98.8%, *P* < 0.001) and dynamic imaging (97.6%, *P* < 0.001).

2. Non-contrast liver MRI as an alternative to gadoxetic acid-enhanced MRI for detection of uveal melanoma liver metastasis

Of 27 patients, 23 patients had 80 hepatic metastases. Overall diagnostic performance for detecting metastases was not significantly different among three MRI sets (*P* = 0.327). The reader-averaged area under the curve (AUC) was 0.951 (95% CI, 0.911–0.991) for NC-MRI, 0.967 (0.937–0.998) for dynamic-MRI, and 0.963 (0.930–0.995) for full-MRI, without significant difference between NC-MRI and full-MRI (*P* = 0.597), and between dynamic-MRI and full-MRI (*P* > 0.999). The sensitivity to detect liver metastasis was 86.9% (78.1–95.7) for NC-MRI, and 91.9% (86.8–97.0) for both dynamic-MRI and full-MRI, without significant difference among them (*P* = 0.166). The PPV was 94.6% (90.0–99.1) for NC-MRI, 94.8% (90.4–99.2) for dynamic-MRI, and 93.6 (89.1–98.2) for full-MRI without significant difference among them (*P* = 0.282).

Conclusions:

The detection sensitivity of HBP for melanoma liver metastasis was 76.0%, which was lower than that of morphologic or dynamic imaging. HBP of gadoxetic acid-enhanced MRI has little advantage in detecting melanoma liver metastases. In fact, NC-MRI is highly accurate for diagnosis of uveal melanoma liver metastasis, compared to full-protocol gadoxetic acid-enhanced MRI. NC-MRI can be an alternative to gadoxetic acid-enhanced MRI for detecting uveal melanoma liver metastases.

Keywords : melanoma; liver; metastasis; magnetic resonance imaging; contrast agent

I. INTRODUCTION

Around 97.0% of melanomas have their primary location identified, which is most frequently the skin, followed by the eye and mucous membrane [1, 2]. Despite the low death rate of melanoma, patients with metastatic melanoma have poor prognosis [3]. In its early stage, melanoma is most often curable simply with surgical removal of the primary tumor [4, 5]. However, in advanced stages, the 5-year survival rate of metastatic melanoma patients goes down to 5.0-19.0% [6]. Thus, for metastatic melanoma, accurate tumor detection and staging are critical to choose the best treatment plan and predict patient prognosis [4, 5].

The liver is the most common initial site of metastasis from melanoma [5, 7-10]. Since patient prognosis heavily depends on liver involvement, it is important to evaluate liver metastasis accurately [8, 11]. The superiority of magnetic resonance imaging (MRI) over other modalities is already well known for liver metastases from other origin tumors such as colorectal cancer, particularly for small metastases less than 1 cm [12-15]. According to previous studies, MRI shows superior sensitivity and specificity for the characterization of hepatic metastases from melanoma over other modalities such as ultrasonography and computed tomography (CT), thus gaining traction as an imaging tool for metastatic melanoma in recent years [16, 17].

There are two types of contrast agents used for liver MRI, the extracellular contrast agent (ECA) and the hepatobiliary agent (HBA) [13]. HBA such as gadoxetic acid offers an additional hepatobiliary phase (HBP) which enables the detection of non-functioning hepatocyte lesions in the background of strongly enhanced normal liver parenchyma [14, 18-20]. Gadoxetic acid-enhanced MRI has shown excellent sensitivity, ranging from 89.9 to 96.3%, to detect colorectal liver metastases [12, 14, 19]. However, there are specific considerations when assessing melanoma liver metastases on MRI. Melanoma liver metastases are often small in size, and show high signal intensity (SI) on T1 weighted imaging (T1WI) due to the T1 shortening effect generated by either the melanin pigment or extracellular met-hemoglobin from intratumoral hemorrhage [5, 9, 17].

Because of these unique signal characteristics, some melanoma liver metastases are not well delineated on HBP, thus HBP might not quite useful for detecting liver metastases from melanoma. However, the signal characteristics and potential additional value of HBP have rarely been studied for melanoma liver metastases.

Therefore, this study was conducted in two parts. The first part aimed to evaluate the imaging findings and detection sensitivity of gadoxetic acid-enhanced MRI for melanoma liver metastases, and to compare these MRI findings according to the primary site of the melanoma. The second part of the study aimed to evaluate the diagnostic performance of different abbreviated MRI sets, including non-contrast MRI (NC-MRI) from a complete gadoxetic acid-enhanced MRI, and to investigate the potential additional value of HBP (hepatobiliary phase imaging) in detecting liver metastasis in patients with uveal melanoma.

II. MATERIALS AND METHODS

The Institutional Review Board approved this retrospective study and required neither patient approval nor informed consent for our review of patient images and medical records.

2.1. Gadoxetic acid-enhanced MRI for detection of liver metastases from melanoma

2.1.1. Study population

From August 2005 to May 2021, patients with liver metastasis from melanoma who underwent liver MRI were consecutively enrolled. Among them, patients without gadoxetic acid-enhanced MRI, with other concurrent malignancies, and with prior systemic treatment were excluded. Patients with inadequate confirmation of liver lesions or imaging artifacts were also excluded. Clinical information including age, sex, pathology, and the primary site of the melanoma was extracted from electronic medical records.

2.1.2. Acquisition of MRI

Liver MRI was performed with either a 3.0-T or a 1.5-T machine. Routine liver MRI sequences included dynamic T1WI, dual-echo spoiled gradient-echo T1-weighted in-phase and opposed-phase imaging, multi-shot and single-shot turbo spin-echo T2-weighted imaging (T2WI), and single-shot echo planar diffusion-weighted imaging (DWI) with b values of 50, 400, and 800 sec/mm^2. Before and after the injection of gadoxetate disodium (Primovist, Bayer Schering Pharma, Berlin, Germany) at a dose of 0.1 mL/kg (0.025 mmol/kg) followed by a 20-mL saline flush at an injection rate of 1 mL/sec, a dynamic fat-suppressed spoiled gradient-echo T1WI was acquired. The bolus-tracking approach was used to calculate the timing of the arterial phase, with an 18-second delay starting from the moment of aortic enhancement. The subsequent dynamic phases, which included the portal and transitional phases, were scanned at intervals of approximately 30 seconds; the time needed for each dynamic phase ranged from 16 to 22 seconds. The HBP was obtained 15–20 minutes after the injection of the contrast agent.

2.1.3. Image analysis

A study coordinator (with 4 years of experience in liver MRI) identified melanoma liver metastases using medical records, histopathologic results, and imaging. The study coordinator chose up to five liver metastases per patient in descending order of size, and measured the size of each lesion. Hepatic metastases were confirmed by histopathologic examination (either biopsy or surgery) or by imaging. On MRI, a liver lesion was considered a metastasis if it showed 1) moderate T2 hyperintensity and T1 hypointensity relative to the liver, with diffuse or peripheral enhancement, or 2) T1 hyperintensity and moderate T2 hyperintensity or hypointensity relative to the liver, regardless of enhancement [21]. For the liver lesions not confirmative for metastasis, follow-up imaging ($\geq$ 12 months) was re-evaluated to determine findings for metastases or disease progression.

Two board-certified abdominal radiologists (dedicated to liver MRI with more than 5 to 10 years of experience) independently evaluated the MR findings of liver metastases. The readers were aware that patients had melanoma with hepatic metastases,

but they were blinded to other clinical data and pathologic findings. The SI of the lesion was evaluated in comparison with the background normal liver. If the lesion showed heterogeneous SI, the SI was determined by its dominant SI. Isointense SI was defined as a lesion with dominant isointensity with a partial hyper- or hypointense portion. If the entire lesion showed the same SI as the surrounding liver, the lesion was considered “not detected”. Since some MRI scans did not include arterial phase subtraction imaging, subtraction imaging was evaluated when available. Positive diffusion restriction was considered for a lesion showing high SI on the highest 'b' value and corresponded low SI on the apparent diffusion coefficient map.

2.1.4. Data and Statistical analysis

Data were presented as numbers and percentages for categorical variables or mean ± standard deviation or median with interquartile range (IQR) for quantitative variables. All statistical analyses were performed on a lesion-based. First, the MR findings of liver metastases were compared according to detection on HBP and according to the primary site of melanoma, respectively. The size of liver metastases was compared using the independent t-test. MR findings were compared using logistic regression with the generalized estimating equation (GEE) considering clustered data due to multiple lesions within a patient. For variables that could not be estimated by GEE, the Chi-square test or Fisher’s exact test was performed.

Second, detection sensitivity for metastases was compared among four different MR imaging sets (morphologic imaging, DWI, dynamic imaging, HBP) using logistic regression with GEE. Morphologic imaging included combined noncontrast T1WI and T2WI, whereas dynamic imaging included contrast-enhanced T1WI (arterial, portal, and transitional phases). Bonferroni correction was applied to adjust *P* values for multiple comparisons. Adjusted *P* values were presented by multiplying the number of comparisons. To compare detection sensitivity among imaging sets, subgroup analyses were performed according to the size of metastasis (≤1 cm vs. >1 cm), and the primary site of the melanoma

(uveal vs. non-uveal).

Lastly, the interobserver agreement of MR interpretation between two readers was evaluated using the bootstrap method to estimate the correlated κ coefficients: κ values < 0.20, poor agreement; 0.21–0.40, fair; 0.41–0.60, moderate; 0.61–0.80, good; and 0.81–1.00, excellent [22]. Statistical analyses were performed using R software, version 4.2.2 *(http://www.R-project.org)*. $P < 0.05$ was considered statistically significant.

2.2. Non-contrast liver MRI as an alternative to gadoxetic acid-enhanced MRI for detection of uveal melanoma liver metastasis

2.2.1. Study population

Patients with melanoma liver metastases who underwent hepatic MRI were consecutively enrolled between August 2005 and May 2021. Patients without gadoxetic acid-enhanced MRI, with poor MR quality, with more than 10 liver lesions on MRI, and with primary origin other than uveal were excluded. Clinical characteristics such as age, gender, pathology, and primary site of the melanoma were extracted from electronic medical records.

2.2.2. Acquisition of MRI

The MRI was acquired using the same method as the first study.

2.2.3. Image analysis

Two board-certified abdominal radiologists (dedicated to liver MRI with more than 5 to 10 years of experience) reviewed three MR imaging sets: NC-MRI (T1-weighted, T2-weighted, and diffusion-weighted imaging), dynamic-MRI (NC-MRI and dynamic phases), and full-MRI (dynamic-MRI and HBP) to detect hepatic metastases based on signal characteristics of the lesion. Dynamic phases included contrast-enhanced T1WI (arterial, portal, and transitional phases). The readers were blinded if patients had melanoma with hepatic metastases, and also to other clinical data and pathologic findings. Hepatic

metastases were confirmed by histopathologic examination (either biopsy or surgery) or by imaging.

2.2.4. Data and Statistical analysis

Data were presented as numbers and percentages for categorical variables or mean ± standard deviation or median with interquartile range (IQR) for quantitative variables. First, overall diagnostic performance of three MR imaging sets (NC-MRI, dynamic-MRI, and full-MRI) for detecting metastases were evaluated using alternative free-response receiver operating characteristic curve analysis. Second, the sensitivity, and positive predictive value (PPV) were also compared among those MR imaging sets using logistic regression with GEE considering clustered data due to multiple lesions within a patient. Bonferroni correction was applied to adjust *P* values for multiple comparisons. Adjusted *P* values were presented by multiplying the number of comparisons. Statistical analyses were performed using R software, version 4.3.3 (http://www.R-project.org), RJafroc, geeglm package. $P < 0.05$ was considered statistically significant.

III. RESULTS

3.1. Gadoxetic acid-enhanced MRI for detection of liver metastases from melanoma

3.1.1. Patient Characteristics

Among 116 patients with liver metastases from melanoma and liver MRI, 49 patients were excluded due to the following reasons: no gadoxetic acid-enhanced MRI (n = 13), concurrent other malignancy (n = 6), prior systemic treatment (n = 19), inadequate confirmation of liver lesions (n = 9) and poor MR image quality (n = 2). Finally, 67 patients with 254 liver metastases were included in this study (Figure. 1; 44 women; mean age ± standard deviation [range], 65.6 ± 13.0 [28–88], years). Liver metastases were confirmed by pathology in 26 patients (22 with biopsy and 4 with surgical resection) and by imaging in 41 patients. Median number of liver metastases per patient was 5 (IQR, 2–5).

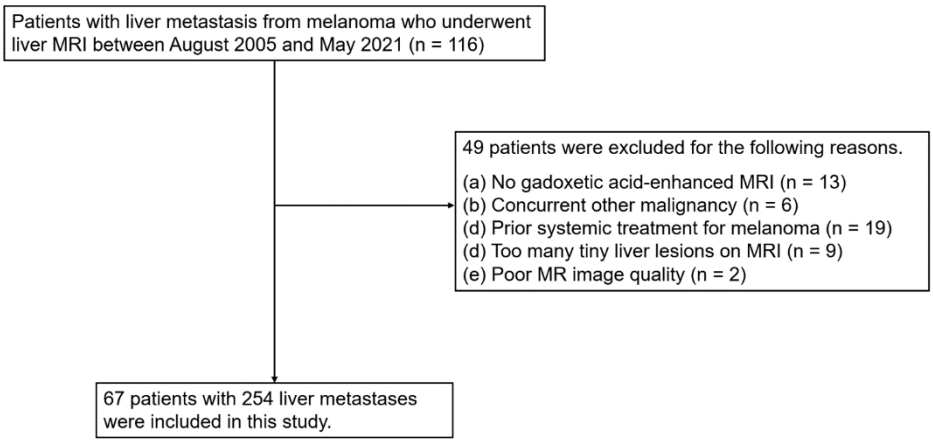

Figure. 1. Patient flow diagram

Table 1. Patient demographics

Variables	Value
Age, year	
Mean ± standard deviation	65.6 ± 13.0 (28–88)
Sex	
Male	23 (34.3)
Female	44 (65.7)
Primary site	
Uvea	57 (85.1)
Liver	2 (3.0)
Skin	2 (3.0)
Rectum/Anus	2 (3.0)
Oro-nasal cavity	2 (3.0)
Esophagus	1 (1.5)
Vulva	1 (1.5)
Confirmation of metastasis	
Pathology	26 (38.8)
Imaging	41 (61.2)
Number of evaluated liver metastases per patient	
Median (Interquartile range)	5 (2–5)

Unless otherwise specified, data are numbers of patients with percentages in parentheses.

3.1.2. Gadoxetic acid-enhanced MRI features of melanoma liver metastases

MR findings according to detection on HBP are summarized in Table 2. Among a total of 254 metastases, 86.2% (219/254) of lesions originated from uveal melanomas. The mean size of the metastases was 1.7 cm, and 43.7% (111/254) of them were ≤ 1 cm. Regarding all metastases, dominant SIs were high on T1WI (68.9%, 175/254) and high on T2WI (55.5%, 141/254), and 65.7% of lesions showed diffusion restriction. On dynamic phases, 80.3% of lesions showed hyperintensity on the arterial phase, and 56.1% of lesions showed arterial enhancement on subtraction imaging. Approximately half of the lesions showed hyperintensity on the portal (55.9%, 142/254) and transitional phases (48.4%, 123/254). To note, 24.0% (61/254) of lesions were not detected on HBP, and residual lesions showed hyperintensity (15.4%, 39/254), isointensity (5.1%, 13/254), or hypointensity (55.5%, 141/254) on HBP.

Regarding MR findings according to detection on HBP, most of the undetected lesions on HBP were of uveal origin (98.4%, 60/61), and 90.2% (55/61) of the undetected lesions were ≤1 cm. Liver metastases detected on HBP showed the following MR findings more frequently than those not detected on HBP: low SI on T1WI, high SI on T2WI, diffusion restriction, arterial enhancement, and hypointensity on the portal and transitional phase (all *Ps* < 0.001). Notably, among 61 undetected lesions on HBP, 98.4% (60/61) showed hyperintensity on T1WI, and 90.2% (55/61) did not show diffusion restriction.

Table 2. MR findings of liver metastases according to the detection on the hepatobiliary phase

	All (n = 254)	Detection (+) (n = 193)	Detection (-) (n = 61)	*P*-value
Primary site				0.002
Uveal	219 (86.2)	159 (82.4)	60 (98.4)	
Non-uveal	35 (13.8)	34 (17.6)	1 (1.6)	
Size (Mean ± SD), cm	1.7 ± 1.9	2.1 ± 2.1	0.6 ± 0.3	<0.001
Size				<0.001
≤1 cm	111 (43.7)	56 (29.0)	55 (90.2)	
>1 cm	143 (56.3)	137 (71.0)	6 (9.8)	
T1-weighted imaging				<0.001
Hypointense	58 (22.8)	57 (29.5)	1 (1.6)	
Isointense	3 (1.2)	3 (1.6)	0 (0)	
Hyperintense	175 (68.9)	115 (59.6)	60 (98.4)	
Not detected	18 (7.1)	18 (9.3)	0 (0)	
T2-weighted imaging				<0.001
Hypointense	41 (16.1)	33 (17.1)	8 (13.1)	
Isointense	1 (0.4)	1 (0.5)	0 (0)	
Hyperintense	141 (55.5)	139 (72.0)	2 (3.3)	
Not detected	71 (28.0)	20 (10.4)	51 (83.6)	
Diffusion restriction				<0.001
Yes	167 (65.7)	161 (83.4)	6 (9.8)	
No	87 (34.3)	32 (16.6)	55 (90.2)	
Arterial phase				<0.001
Hypointense	37 (14.6)	37 (19.2)	0 (0)	
Isointense	2 (0.8)	2 (1.0)	0 (0)	
Hyperintense	204 (80.3)	152 (78.8)	52 (85.2)	
Not detected	11 (4.3)	2 (1.0)	9 (14.8)	

Arterial phase subtraction*				<0.001
Enhancement	133 (56.1)	121 (68.4)	12 (20.0)	
No enhancement	104 (43.9)	56 (31.6)	48 (80.0)	
Portal phase				<0.001
Hypointense	74 (29.1)	72 (37.3)	2 (3.3)	
Isointense	12 (4.7)	12 (6.2)	0 (0)	
Hyperintense	142 (55.9)	98 (50.8)	44 (72.1)	
Not detected	26 (10.2)	11 (5.7)	15 (24.6)	
Transitional phase				<0.001
Hypointense	91 (35.8)	88 (45.6)	3 (4.9)	
Isointense	6 (2.4)	6 (3.1)	0 (0)	
Hyperintense	123 (48.4)	81 (42.0)	42 (68.9)	
Not detected	34 (13.4)	18 (9.3)	16 (26.2)	
Hepatobiliary phase				NA
Hypointense	141 (55.5)	141 (73.1)		
Isointense	13 (5.1)	13 (6.7)		
Hyperintense	39 (15.4)	39 (20.2)		
Not detected	61 (24.0)		61 (100)	

*A total of 237 lesions were evaluated on arterial subtraction imaging, because arterial subtraction imaging was not available for 17 lesions from 4 patients.
SD, standard deviation; NA, not applicable

MR findings according to the primary site of melanoma are summarized in Table 3. Metastases of non-uveal origin showed the following MR findings more frequently than those of uveal origin: low SI on T1WI, high SI on T2WI, diffusion restriction, arterial enhancement on subtraction imaging, and low SI on HBP ($Ps \leq 0.019$). Lesion size and SIs on the arterial, portal, and transitional phases did not significantly differ according to the primary site ($Ps > 0.05$). Representative cases are presented in Figures 2–3.

Table 3. MR findings of liver metastases according to the primary site of melanoma

	Uveal (n = 219)	Non-uveal (n = 35)	*P*-value
Size (Mean ± SD), cm	1.7 ± 1.7	2.2 ± 2.9	0.182
Size			0.242
≤1 cm	99 (45.2)	12 (34.3)	
>1 cm	120 (54.8)	23 (65.7)	
T1-weighted imaging			<0.001
Hypointense	46 (21.0)	12 (34.3)	
Isointense	3 (1.4)	0 (0)	
Hyperintense	158 (72.1)	17 (48.6)	
Not detected	12 (5.5)	6 (17.1)	
T2-weighted imaging			<0.001
Hypointense	38 (17.4)	3 (8.6)	
Isointense	1 (0.5)	0 (0)	
Hyperintense	110 (50.2)	31 (88.6)	
Not detected	70 (32.0)	1 (2.9)	
Diffusion restriction			0.019
Yes	135 (61.6)	32 (91.4)	
No	84 (38.4)	3 (8.6)	
Arterial phase			0.126
Hypointense	28 (12.8)	9 (25.7)	
Isointense	2 (0.9)	0 (0)	
Hyperintense	178 (81.3)	26 (74.3)	
Not detected	11 (5.0)	0 (0)	
Arterial phase subtraction*			<0.001
Enhancement	103 (51.0)	30 (85.7)	
No enhancement	99 (49.0)	5 (14.3)	
Portal phase			0.450
Hypointense	58 (26.5)	16 (45.7)	
Isointense	9 (4.1)	3 (8.6)	
Hyperintense	130 (59.4)	12 (34.3)	
Not detected	22 (10.0)	4 (11.4)	
Transitional phase			0.432
Hypointense	72 (32.9)	19 (54.3)	
Isointense	5 (2.3)	1 (2.9)	
Hyperintense	115 (52.5)	8 (22.9)	
Not detected	27 (12.3)	7 (20.0)	
Hepatobiliary phase			<0.001
Hypointense	112 (51.1)	29 (82.9)	
Isointense	13 (5.9)	0 (0)	
Hyperintense	34 (15.5)	5 (14.3)	
Not detected	60 (27.4)	1 (2.9)	

*A total of 237 lesions were evaluated on arterial subtraction imaging, because arterial subtraction imaging was not available for 17 lesions from 4 patients.
SD, standard deviation

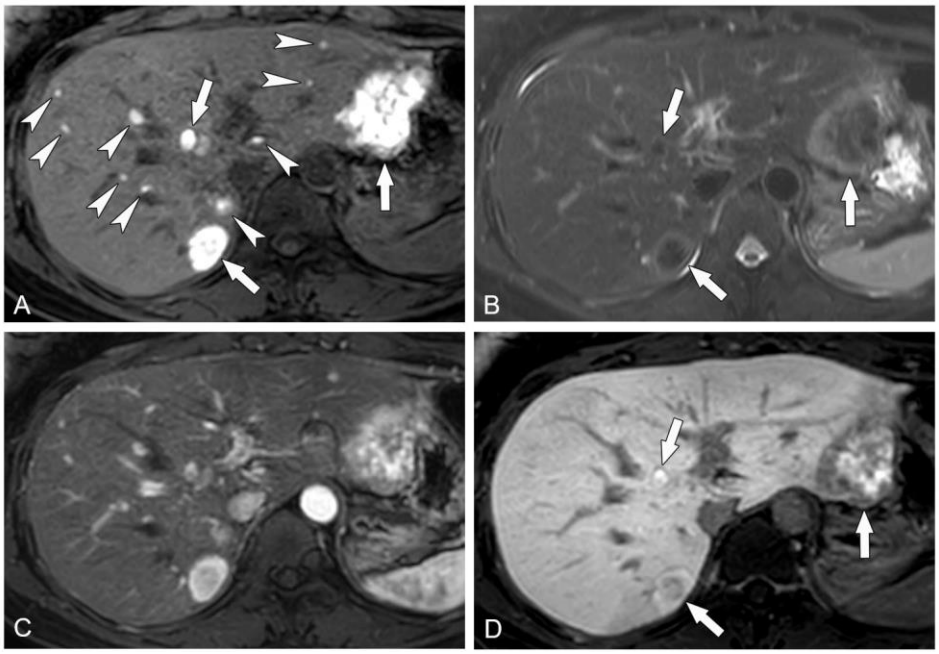

Figure. 2. Gadoxetic acid-enhanced MRI in a 53-year-old woman with liver metastases from uveal (choroidal) melanoma

Axial precontrast T1WI (A), fat-suppressed T2WI (B), arterial phase T1WI (C), and hepatobiliary phase (D) show multiple hepatic metastases. Among these lesions, three metastases are detected (arrows) with low SI on fat-suppressed T2WI (B), and heterogeneous high SI on hepatobiliary phase (D). On precontrast T1WI (A) and arterial phase T1WI (C), multiple hyperintense lesions are additionally detected, suggestive of metastases (arrowheads).

T1WI, T1-weighted image; T2WI, T2-weighted image; DWI, diffusion-weighted image; HBP, hepatobiliary phase; SI, signal intensity

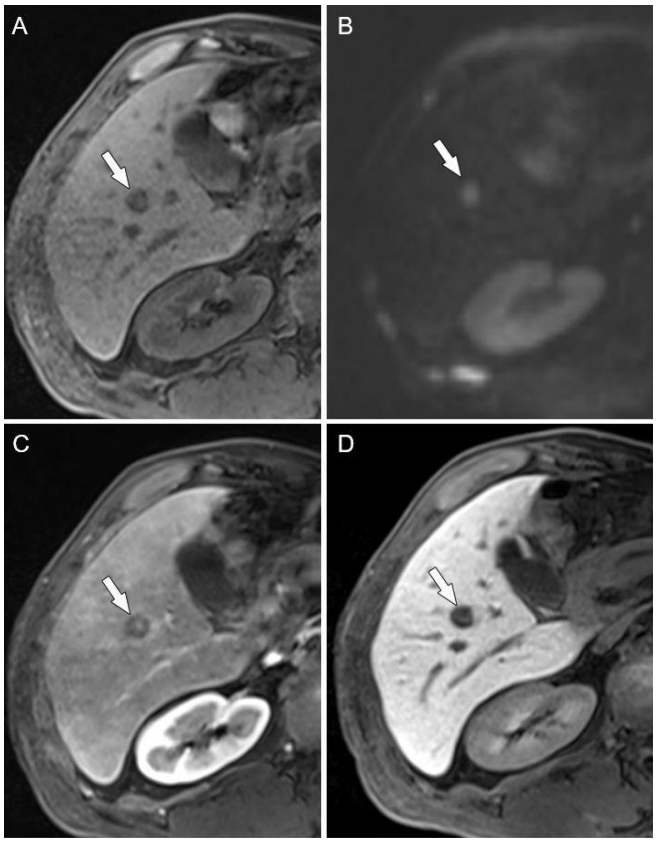

Figure. 3. Gadoxetic acid-enhanced MRI in a 59-year-old man with liver metastases from non-uveal (oral mucosal) melanoma

A 1.2-cm metastasis in the right inferior liver (arrows) shows low SI on precontrast T1WI (A), high SI on DWI (b = 800 s/mm^2) (B), low SI with peripheral enhancement on portal phase T1WI (C), and low SI on hepatobiliary phase (D).

T1WI, T1-weighted image; T2WI, T2-weighted image; DWI, diffusion-weighted image; HBP, hepatobiliary phase; SI, signal intensity

3.1.3. Comparison of detection sensitivity for liver metastasis among different MR sequences

Detection sensitivity was compared among four different MR imaging sets (morphologic imaging, DWI, dynamic imaging, and HBP), with the results presented in Table 4 and 5. For all metastases, the detection sensitivity of HBP (76.0%) was significantly lower than morphologic (98.8%, $P < 0.001$), and dynamic imaging (97.6%, $P < 0.001$). On the other hand, the detection rate of HBP was significantly higher than that of DWI (65.7%, $P = 0.006$). When compared with other imaging sets, no lesion was additionally detected on HBP.

Table 4. Comparison of detection sensitivity of MR imaging sets according to lesion size and primary site

	Detection sensitivity			
	Morphologic	DWI	Dynamic	HBP
All lesions (n = 254)	251 (98.8)	167 (65.7)	248 (97.6)	193 (76.0)
Lesion size				
≤1 cm (n = 111)	109 (98.2)	43 (38.7)	105 (94.6)	56 (50.5)
>1 cm (n = 143)	142 (99.3)	124 (86.7)	143 (100.0)	137 (95.8)
***P*-value** †	0.144	<0.001	0.694	<0.001
Primary site				
Uveal (n = 219)	216 (98.6)	135 (61.6)	213 (97.3)	159 (72.6)
Non-uveal (n = 35)	35 (100.0)	32 (91.4)	35 (100.0)	34 (97.1)
***P*-value** ‡	0.235	<0.001	0.104	<0.001

Data are numbers of detected lesions with percentages in parentheses.
†*P* values are obtained by comparing the detection sensitivity of each imaging set according to lesion size.
‡*P* values are obtained by comparing the detection sensitivity of each imaging set according to the primary site of the melanoma.
'Morphologic' indicates combined T1WI and T2WI, and 'Dynamic' indicates a combination of arterial, portal, and transitional phases.

T1WI, T1-weighted imaging; T2WI, T2-weighted imaging; DWI, diffusion-weighted imaging; HBP, hepatobiliary phase

Table 5. Comparison of detection sensitivity between HBP and each other imaging set

	***P*-value ***		
	Morphologic vs. HBP	DWI vs. HBP	Dynamic vs. HBP
All lesions (n = 254)	<0.001	0.006	<0.001
Lesion size			
≤1 cm (n = 111)	<0.001	0.102	<0.001
>1 cm (n = 143)	0.300	0.096	0.054
Primary site			
Uveal (n = 219)	<0.001	0.012	<0.001
Non-uveal (n = 35)	>0.999	0.738	>0.999

**P* values are obtained by comparing the detection sensitivity of HBP and each imaging set. These are adjusted *P* values using Bonferroni correction.
'Morphologic' indicates combined T1WI and T2WI, and 'Dynamic' indicates a combination of arterial, portal, and transitional phases.

T1WI, T1-weighted imaging; T2WI, T2-weighted imaging; DWI, diffusion-weighted imaging; HBP, hepatobiliary phase

In the subgroup analysis according to lesion size, metastases larger than 1 cm showed better detection sensitivity than smaller lesions on DWI (86.7% vs. 38.7%, $P < 0.001$) and HBP (95.8% vs. 50.5%, $P < 0.001$), but the detection sensitivity according to lesion size was not significantly different on morphologic ($P = 0.144$), and dynamic imaging ($P = 0.694$). For metastases larger than 1 cm, the detection sensitivity did not significantly differ between HBP and other imaging sets (*Ps* > 0.05). For smaller metastases (≤ 1 cm), the detection sensitivity of HBP (50.5%) was significantly lower than morphologic (98.2%, $P < 0.001$) and dynamic imaging (94.6%, $P < 0.001$).

Regarding the primary site of melanoma, the detection sensitivity for metastases from uveal melanoma was significantly lower than those from non-uveal melanoma on DWI (61.6% vs. 91.4%, $P < 0.001$) and HBP (72.6% vs. 97.1%, $P < 0.001$). For metastases of uveal melanoma, the detection sensitivity among the four MR imaging sets showed similar trends to the results found with all metastases: the sensitivity of HBP (72.6%) was

significantly lower than morphologic (98.6%, $P < 0.001$) and dynamic imaging (97.3%, $P < 0.001$), but was significantly higher than DWI (61.6%, $P = 0.012$). On the other hand, for metastases from non-uveal melanoma, the detection sensitivity did not significantly differ among the four imaging sets (*Ps* > 0.05).

Interobserver agreement for MR interpretation is summarized in Table 6. The interobserver agreement was lowest for arterial subtraction imaging (κ = 0.500). HBP showed good interobserver agreement (κ = 0.712). For the other sequences, overall interobserver agreement was good to excellent (κ, 0.684–0.868).

Table 6. Inter-reader agreement of the MRI evaluation

MR Sequence	κ statistics (95% confidence interval)
T1-weighted imaging	0.743 (0.622-0.863)
T2-weighted imaging	0.734 (0.655-0.813)
Diffusion-weighted imaging	0.868 (0.784-0.952)
Arterial phase	0.684 (0.533-0.835)
Arterial phase subtraction	0.500 (0.355-0.646)
Portal phase	0.753 (0.676-0.830)
Transitional phase	0.772 (0.691-0.852)
Hepatobiliary phase	0.712 (0.643-0.780)

3.2. Non-contrast liver MRI as an alternative to gadoxetic acid-enhanced MRI for detection of uveal melanoma liver metastasis

3.2.1. Patient Characteristics

Among 116 patients with liver metastases from melanoma and liver MRI, 89 patients were excluded due to the following reasons: no gadoxetic acid-enhanced MRI (n = 13), concurrent other malignancy (n = 6), poor MR image quality (n = 2), >10 liver lesions on MRI (n = 57), and primary origin other than uvea (n = 11). Total 27 patients were finally included in the study. Of 27 patients, 23 patients had 80 hepatic metastases (Figure. 4; 14 women; mean age ± standard deviation [range], 64.7 ± 13.7 [28–88], years). Liver metaseses were confirmed by pathology in 13 patients and by imaging in 14 patients. Median number of liver metastases per patient was 2 (IQR, 1–5).

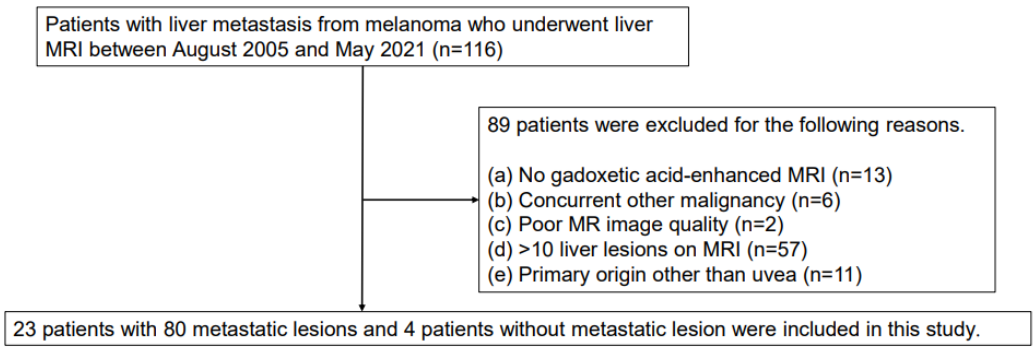

Figure. 4. Patient flow diagram

Table 7. Patient demographics

Variables	Value
Age, year	
Mean ± standard deviation [6]	64.7 ± 13.7 (28–88)
Sex	
Male	13 (48.1)
Female	14 (51.9)
Confirmation of metastasis	
Pathology	13 (48.1)
Imaging	14 (51.9)
Number of evaluated liver metastases per patient	
Median (Interquartile range)	2 (1–5)

Unless otherwise specified, data are numbers of patients with percentages in parentheses.

3.2.2. Diagnostic performance of abbreviated MRI sets to detect uveal melanoma liver metastases

Overall diagnostic performances for detecting metastases for each MR imaging set are summarized in Table 8. The overall diagnostic performance for detecting metastases was not significantly different among the three MRI sets ($P = 0.327$). The reader-averaged area under the curve (AUC) was 0.951 (95% CI, 0.911-0.991) for NC-MRI, 0.967 (0.937-0.998) for dynamic-MRI, and 0.963 (0.930-0.995) for full-MRI, with no significant difference between NC-MRI and full-MRI ($P = 0.597$) or between dynamic-MRI and full-MRI ($P > 0.999$). The AUC value for Reader 1 was 0.976 for dynamic MRI and 0.942 for NC-MRI, with the dynamic MRI being statistically significantly higher than the NC-MRI ($P = 0.033$), but no significant difference between NC-MRI and full-MRI ($P = 0.183$) or between dynamic-MRI and full-MRI ($P > 0.999$). AUC of reader 2 showed no significant difference among the three MRI sets (Ps > 0.999).

Table 8. Overall diagnostic performance for detection of hepatic metastases

		AUC	
MRI imaging set	Reader-averaged (95% CI)	Reader 1	Reader 2
NC-MRI	0.951 (0.911-0.991)	0.942	0.96
Dynamic-MRI	0.967 (0.937-0.998)	0.976*	0.958
Full-MRI	0.963 (0.93-0.995)	0.967	0.958

Numbers in parenthesis are 95% confidence intervals.
*The AUC value is significantly higher than that of NC-MRI (P = 0.033).

AUC, area under curve; MRI, magnetic resonance imaging; NC, noncontrast

The sensitivities for detection of hepatic metastases are summarized in Table 9. The sensitivity for detecting liver metastases was 86.9% (78.1–95.7) for NC-MRI, and 91.9% (86.8–97.0) for both dynamic-MRI and full-MRI. There was no significant difference in sensitivity among the reader-averaged MRI imaging sets (P = 0.166), and no significant differences were found in any comparisons for each individual reader (Ps $\geq$ 0.05). Representative case is presented in Figures 5.

Table 9. Sensitivities for detection of hepatic metastases

		Sensitivity (%)	
MRI imaging set	Reader-averaged (95% CI)	Reader 1	Reader 2
NC-MRI	86.9 (78.1-95.7)	83.8 (67/80)	90.0 (72/80)
Dynamic-MRI	91.9 (86.8-97.0)	93.8 (75/80)	90.0 (72/80)
Full-MRI	91.9 (86.8-97.0)	93.8 (75/80)	90.0 (72/80)

Numbers in parenthesis are the number of lesions, which were used for calculating the percentages. Percentages were rounded.
There were no significant differences among all MRI imaging sets ($Ps \geq 0.05$)

CI, confidence interval; MRI, magnetic resonance imaging; NC, noncontrast

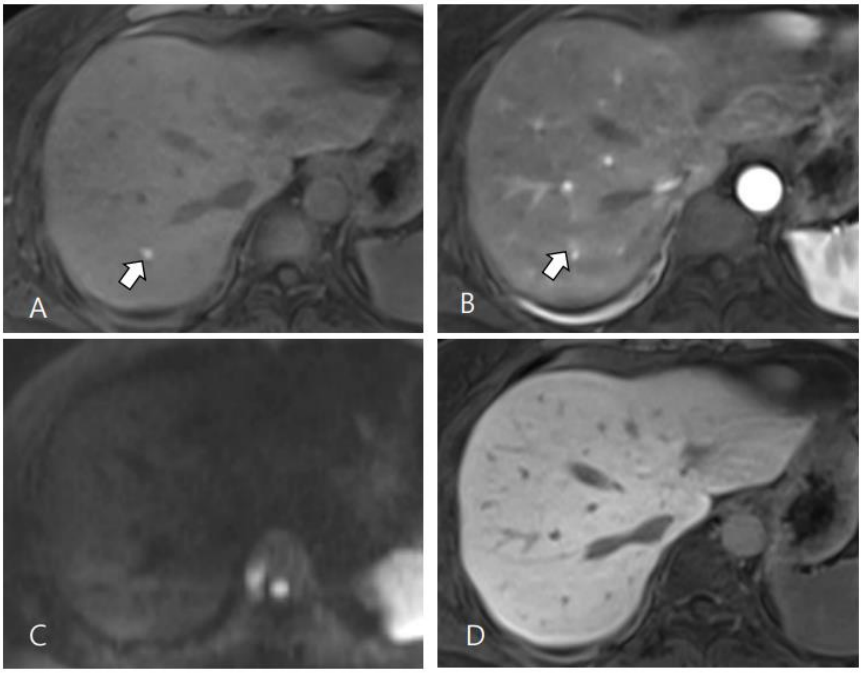

Figure. 5. Gadoxetic acid-enhanced MRI in a 78-year-old woman with liver metastases from uveal (choroidal) melanoma

Gadoxetic acid-enhanced MRI shows a tiny metastasis in the liver S7 (arrow). This lesion shows high signal intensity on axial precontrast T1WI (A), and arterial phase T1WI (B), but itis barely detectable on DWI (C) and HBP (D). A total of 8 metastases (not seen) were accurately identified on NC-MRI as well as other MR imaging sets.

T1WI, T1-weighted image; DWI, diffusion-weighted imaging; HBP, hepatobiliary phase; NC, noncontrast

The PPVs for detection of hepatic metastases are summarized in Table 10. The PPV was 94.6% (90.0–99.1) for NC-MRI, 94.8% (90.4–99.2) for dynamic-MRI, and 93.6% (89.1–98.2) for full-MRI. There was no significant difference in PPVs among the reader-averaged MRI imaging sets ($P = 0.282$), and no significant differences were found in any comparisons for each individual reader (Ps ≥ 0.05).

Table 10. PPVs for detection of hepatic metastases

	PPV (%)		
MRI imaging set	Reader-averaged (95% CI)	Reader 1	Reader 2
NC-MRI	94.6 (90.0-99.1)	97.1 (67/69)	92.3 (72/78)
Dynamic-MRI	94.8 (90.4-99.2)	97.4 (75/77)	92.3 (72/78)
Full-MRI	93.6 (89.1-98.2)	94.9 (75/79)	92.3 (72/78)

Numbers in parenthesis are the number of lesions, which were used for calculating the percentages. Percentages were rounded.
There were no significant differences among all MRI imaging sets ($Ps \geq 0.05$)

PPV, positive predictive value; CI, confidence interval; MRI, magnetic resonance imaging; NC, noncontrast

IV. DISCUSSION

It is generally assumed that the use of liver-specific contrast agents for liver MRI can improve the detection of liver metastasis due to the high lesion-to-liver contrast on HBP [12, 13]. However, little research has been conducted on whether this also applies to the liver metastasis of melanoma, which can show unique MR signal characteristics.

4.1. Gadoxetic acid-enhanced MRI for detection of liver metastases from melanoma

Our first study demonstrated the gadoxetic acid-enhanced MRI findings of liver metastases from melanoma, focusing on the usefulness of HBP. On HBP, 55.5% of liver metastases showed hypointensity, 20.5% showed iso- to hyperintensity, and 24.0% were not detected. The metastases which could be detected on HBP were more frequently of non-uveal origin, larger in size, and showed T1 hypointensity, T2 hyperintensity, diffusion restriction, and arterial enhancement compared to those not detected on HBP. The overall detection rate of HBP was significantly higher than DWI, but lower than morphologic (combined T1WI and

T2WI), or dynamic imaging.

Hepatic metastases from other origins typically show rim enhancement on early post-contrast phases, with incomplete centripetal progression on the portal venous and delayed phases [23, 24]. On HBP, most liver metastases from malignancies other than melanoma typically demonstrate global or peripheral hypointense SI as they do not have functional hepatocytes [14, 25]. However, the high T1 SI of melanoma liver metastases, which is frequently observed for metastases from pigmented uveal melanoma [21, 26], can preclude the detection of metastasis on HBP. Our study revealed that most undetected metastases on HBP (60/61) were hyperintense on T1WI. Remarkably, no lesion was additionally detected on HBP compared to other sequences. Generally, ECA offers superior quality of arterial phase than HBA, mainly due to frequent respiratory motion artifacts and a lower gadolinium dose of HBA[27]. In addition, scan times are possibly longer with HBA, since the final post-contrast phase is obtained approximately 15 to 20 minutes after HBA injection [28]. Based on our results, HBA may not be preferred to ECA for detecting liver metastasis from melanoma.

DWI alone revealed the lowest detection sensitivity (65.7%) for melanoma liver metastasis among MR sequences, although its detection sensitivity was relatively higher for larger metastases and metastases from non-uveal melanoma. A previous study reported a sensitivity of 53.0–59.0% for DWI when detecting uveal melanoma liver metastasis and also suggested that DWI did not provide additional benefits to morphologic-dynamic imaging for the detection of melanoma liver metastasis [21]. This discrepancy between the usefulness of DWI for detecting melanoma liver metastasis and other metastases such as colorectal/or neuroendocrine liver metastasis might be related to how the melanin component affects T2WI and DWI [21]. Notably, noncontrast morphologic imaging (T1WI and T2WI) showed excellent detection sensitivity, which is higher than DWI and HBP in our study. A previous study comparing the detection rate of MRI and positron emission tomography also showed perfect sensitivity of unenhanced T1WI and T2WI for detecting melanoma liver metastasis [29]. These results are encouraging because noncontrast liver

MRI can be used as a surveillance or diagnosis tool for melanoma liver metastasis.

In this study, MR findings of liver metastases were compared according to the primary site of melanoma. As results, liver metastases from non-uveal melanoma showed less T1 hyperintensity, and more T2 hyperintensity, diffusion restriction, arterial enhancement and HBP hypointensity than metastases from uveal melanoma. Therefore, MR features of liver metastases from non-uveal melanoma are more similar to the typical appearance of liver metastases other than melanoma, and 97.1% of metastases from non-uveal melanoma were detected on HBP. These differences are probably because uveal melanomas are more commonly melanotic than non-uveal melanomas such as cutaneous melanomas [30]. Therefore, special consideration based on the knowledge of unique MR features is needed to interpret liver MRI for uveal melanoma metastases. However, most metastases included in this study originated from uveal melanoma, thus further studies including large number of metastases from non-uveal melanoma are warranted to generalize our results.

There are several limitations to the first study. First, data were collected retrospectively, which may have inevitably resulted in a selection bias. It is important to highlight the substantial difference in the ratio of uveal to non-uveal cases, with non-uveal cases being very few. Furthermore, there is a significant selection bias caused by the common practice in the institution of evaluating liver MRI for uveal melanoma patients, resulting in a substantial accumulation of uveal cases in the dataset. Second, not all metastases were confirmed by pathology. However, a complete pathological evaluation of melanoma liver metastasis is clinically impossible, and we believe that the MRI characteristics and follow-up imaging might be sufficient for the diagnosis of metastases. Finally, each MR sequence was not reviewed separately, thus interpretation of each sequence might be influenced by the findings of the other sequence. Although we chose this study design to comprehensively evaluate the lesion-by-lesion signal characteristics of melanoma liver metastasis on gadoxetic acid-enhanced MRI, the detection rate of each sequence might be overestimated.

4.2. Non-contrast liver MRI as an alternative to gadoxetic acid-enhanced MRI for detection of uveal melanoma liver metastasis

The background for conducting the second part of this study stems from the limitations observed in the first part. In the first study, each MR sequence was reviewed separately, and pre-identified lesions were assessed, which may not accurately reflect real-world diagnostic conditions and could potentially lead to an overestimation of sensitivity. Additionally, uveal melanoma presents distinct MR signal characteristics compared to non-uveal melanoma [31]. Therefore, it is essential to evaluate the performance of gadoxetic acid-enhanced MRI specifically in uveal melanoma cases. This second study aims to address these issues by considering the comprehensive diagnostic performance of gadoxetic acid-enhanced MRI in uveal melanoma and to mitigate the potential biases identified in the first study.

The findings of this second study indicate that the overall diagnostic performance for detecting metastases did not significantly differ among the three MRI sets. The AUC for NC-MRI was 0.951, for dynamic-MRI was 0.967, and for full-MRI was 0.963. There was no significant difference in AUC when comparing NC-MRI to either dynamic-MRI or full-MRI. Sensitivity and PPVs for detecting liver metastases was also high across all sets, with no significant differences among them.

Therefore, NC-MRI alone is highly accurate for the diagnosis of uveal melanoma liver metastasis, comparable to full-protocol gadoxetic acid-enhanced MRI. In addition, there was no incremental value of HBP compared to dynamic-MRI for detecting uveal melanoma liver metastasis. Using NC-MRI offers the advantage of eliminating the need for contrast agents, thereby reducing the burden on patients and shortening scan times [32]. Therefore, NC-MRI could be effectively used for liver metastasis surveillance in patients with uveal melanoma.

The second study has several limitations. Similar to the first study, the retrospective nature of data collection and the absence of pathological confirmation for all

metastases may have introduced some bias. However, due to the impracticality of complete pathological evaluations for melanoma liver metastases, MRI characteristics and follow-up imaging are considered sufficient for diagnosis. Another limitation of the second study is the small sample size. This appears to be related to the exclusion of patients with more than 10 metastatic lesions, given that uveal melanoma metastases are frequently multiple. This exclusion was implemented to facilitate image review and lesion matching. To generalize our findings, further research with a larger number of patients is needed.

V. CONCLUSION

In conclusion, the detection sensitivity of HBP for melanoma liver metastases was 76.0%, which was lower than that of morphologic or dynamic imaging. HBP of gadoxetic acid-enhanced MRI has little value for detecting melanoma liver metastases, and particularly less for metastases from uveal melanoma. In fact, NC-MRI is highly accurate for diagnosis of uveal melanoma liver metastasis, compared to full-protocol gadoxetic acid-enhanced MRI. NC-MRI can be an alternative to gadoxetic acid-enhanced MRI for detecting uveal melanoma liver metastases.

REFERENCES

1. J. F. Scott and M. R. Gerstenblith, "Melanoma of unknown primary," *Exon Publications*, pp. 99-116, 2018.
2. N. Takahashi, K. Tajiri, K. Kagoyana, S. Tanaka, and I. Yasuda, "CD8 Positive T lymphocyte infiltration of liver metastases of uveal melanoma: a case report," *Frontiers in Oncology*, vol. 11, p. 672660, 2021.
3. G. Petralia *et al.*, "Whole-body diffusion-weighted imaging: is it all we need for detecting metastases in melanoma patients?," (in eng), *Eur Radiol*, vol. 23, no. 12, pp. 3466-76, Dec 2013, doi: 10.1007/s00330-013-2968-x.
4. A. Schraag *et al.*, "Baseline clinical and imaging predictors of treatment response and overall survival of patients with metastatic melanoma undergoing immunotherapy," (in eng), *Eur J Radiol*, vol. 121, p. 108688, Dec 2019, doi: 10.1016/j.ejrad.2019.108688.
5. M. Barat *et al.*, "CT, MRI and PET/CT features of abdominal manifestations of cutaneous melanoma: a review of current concepts in the era of tumor-specific therapies," (in eng), *Abdom Radiol (NY)*, vol. 46, no. 5, pp. 2219-2235, May 2021, doi: 10.1007/s00261-020-02837-4.
6. C. Durot, S. Mulé, P. Soyer, A. Marchal, F. Grange, and C. Hoeffel, "Metastatic melanoma: pretreatment contrast-enhanced CT texture parameters as predictive biomarkers of survival in patients treated with pembrolizumab," (in eng), *Eur Radiol*, vol. 29, no. 6, pp. 3183-3191, Jun 2019, doi: 10.1007/s00330-018-5933-x.
7. M. Patel *et al.*, "Characterization of computed tomography scan abnormalities in patients with biopsy-proven hepatic metastases from uveal melanoma," (in eng), *Arch Ophthalmol*, vol. 129, no. 12, pp. 1576-82, Dec 2011, doi: 10.1001/archophthalmol.2011.263.
8. K. Sofue, U. Tateishi, M. Tsurusaki, Y. Arai, N. Yamazaki, and K. Sugimura, "MR imaging of hepatic metastasis in patients with malignant melanoma: evaluation of suspected lesions screened at contrast-enhanced CT," (in eng), *Eur J Radiol*, vol. 81, no. 4, pp. 714-8, Apr 2012, doi: 10.1016/j.ejrad.2011.01.123.
9. T. Ramtohul *et al.*, "Prognostic implications of MRI melanin quantification and cytogenetic abnormalities in liver metastases of uveal melanoma," *Cancers*, vol. 13, no. 11, p. 2728, 2021.
10. S. Yavuzyigitoglu *et al.*, "Radiological Patterns of Uveal Melanoma Liver Metastases in Correlation to Genetic Status," (in eng), *Cancers (Basel)*, vol. 13, no. 21, Oct 22 2021, doi: 10.3390/cancers13215316.
11. P. N. Dayani, J. E. Gould, D. B. Brown, K. V. Sharma, G. P. Linette, and J. W. Harbour, "Hepatic metastasis from uveal melanoma: angiographic pattern predictive of survival after hepatic arterial chemoembolization," (in eng), *Arch Ophthalmol*, vol. 127, no. 5, pp. 628-32, May 2009, doi: 10.1001/archophthalmol.2009.45.
12. V. Granata *et al.*, "Diagnostic performance of gadoxetic acid–enhanced liver MRI versus multidetector CT in the assessment of colorectal liver metastases compared to hepatic resection," *BMC gastroenterology*, vol. 19, no. 1, pp. 1-11, 2019.
13. C. L. Welle, F. F. Guglielmo, and S. K. Venkatesh, "MRI of the liver: choosing the right contrast agent," *Abdominal radiology*, vol. 45, pp. 384-392, 2020.
14. A. D. Karaosmanoglu, M. R. Onur, M. N. Ozmen, D. Akata, and M. Karcaaltincaba, "Magnetic Resonance Imaging of Liver Metastasis," (in eng), *Semin Ultrasound CT MR*, vol. 37, no. 6, pp. 533-548, Dec 2016, doi: 10.1053/j.sult.2016.08.005.
15. S. Poetter-Lang *et al.*, "Quantification of liver function using gadoxetic acid-enhanced

MRI," *Abdominal Radiology,* vol. 45, pp. 3532-3544, 2020.
16. J. H. Francis, F. Catalanotti, J. Landa, C. A. Barker, A. N. Shoushtari, and D. H. Abramson, "Hepatic abnormalities identified by staging MRI and accuracy of MRI of patients with uveal melanoma," (in eng), *Br J Ophthalmol,* vol. 103, no. 9, pp. 1266-1271, Sep 2019, doi: 10.1136/bjophthalmol-2018-312612.
17. T. Maeda, U. Tateishi, S. Suzuki, Y. Arai, E. E. Kim, and K. Sugimura, "Magnetic resonance screening trial for hepatic metastasis in patients with locally controlled choroidal melanoma," (in eng), *Jpn J Clin Oncol,* vol. 37, no. 4, pp. 282-6, Apr 2007, doi: 10.1093/jjco/hym018.
18. R. Balasubramanya *et al.*, "Imaging of ocular melanoma metastasis," (in eng), *Br J Radiol,* vol. 89, no. 1065, p. 20160092, Sep 2016, doi: 10.1259/bjr.20160092.
19. R. Bhayana, V. Baliyan, H. Kordbacheh, and A. Kambadakone, "Hepatobiliary phase enhancement of liver metastases on gadoxetic acid MRI: assessment of frequency and patterns," *European Radiology,* vol. 31, pp. 1359-1366, 2021.
20. C. Burke, L. A. Grant, V. Goh, and N. Griffin, "The role of hepatocyte-specific contrast agents in hepatobiliary magnetic resonance imaging," in *Seminars in Ultrasound, CT and MRI*, 2013, vol. 34, no. 1: Elsevier, pp. 44-53.
21. M. Wagner *et al.*, "Diffusion-weighted MRI for uveal melanoma liver metastasis detection," (in eng), *Eur Radiol,* vol. 25, no. 8, pp. 2263-73, Aug 2015, doi: 10.1007/s00330-015-3662-y.
22. S. Vanbelle and A. Albert, "A bootstrap method for comparing correlated kappa coefficients," *Journal of Statistical Computation and Simulation,* vol. 78, no. 11, pp. 1009-1015, 2008.
23. I. M. Danet *et al.*, "Spectrum of MRI appearances of untreated metastases of the liver," (in eng), *AJR Am J Roentgenol,* vol. 181, no. 3, pp. 809-17, Sep 2003, doi: 10.2214/ajr.181.3.1810809.
24. J. Martin *et al.*, "Colorectal liver metastases: Current management and future perspectives," *World journal of clinical oncology,* vol. 11, no. 10, p. 761, 2020.
25. Y.-Y. Kim, M.-S. Park, K. S. Aljoqiman, J.-Y. Choi, and M.-J. Kim, "Gadoxetic acid-enhanced magnetic resonance imaging: Hepatocellular carcinoma and mimickers," *Clinical and molecular hepatology,* vol. 25, no. 3, p. 223, 2019.
26. P. Mariani *et al.*, "Surgical management of liver metastases from uveal melanoma: 16 years' experience at the Institut Curie," (in eng), *Eur J Surg Oncol,* vol. 35, no. 11, pp. 1192-7, Nov 2009, doi: 10.1016/j.ejso.2009.02.016.
27. D. W. Kim *et al.*, "Diagnostic performance of MRI for HCC according to contrast agent type: a systematic review and meta-analysis," *Hepatology International,* vol. 14, pp. 1009-1022, 2020.
28. C. L. Welle, F. F. Guglielmo, and S. K. Venkatesh, "MRI of the liver: choosing the right contrast agent," (in eng), *Abdom Radiol (NY),* vol. 45, no. 2, pp. 384-392, Feb 2020, doi: 10.1007/s00261-019-02162-5.
29. N. Ghanem *et al.*, "Detectability of liver metastases in malignant melanoma: prospective comparison of magnetic resonance imaging and positron emission tomography," (in eng), *Eur J Radiol,* vol. 54, no. 2, pp. 264-70, May 2005, doi: 10.1016/j.ejrad.2004.07.005.
30. A. R. Keraliya *et al.*, "Extracutaneous melanomas: a primer for the radiologist," (in eng), *Insights Imaging,* vol. 6, no. 6, pp. 707-17, Dec 2015, doi: 10.1007/s13244-015-0427-8.
31. C. Bellerive, E. Ouellet, A. Kamaya, and A. D. Singh, "Liver imaging techniques: recognition of uveal melanoma metastases," *Ocular Oncology and Pathology,* vol. 4, no.

4, pp. 254-260, 2018.
32. N. Schieda *et al.*, "Adverse events to the gadolinium-based contrast agent gadoxetic acid: systematic review and meta-analysis," *Radiology*, vol. 297, no. 3, pp. 565-572, 2020.

Abstract in Korean

흑색종에서 간 전이 진단을 위한 자기공명영상의 포괄적 분석

목적:

본 연구의 목적은 흑색종 간 전이를 진단하기 위한 자기공명영상 프로토콜에 대한 포괄적인 분석을 하는 것이다.

방법:

1. 흑색종 간 전이 진단을 위한 가독세틱산 조영증강 자기공명영상의 유용성

본 후향적 연구는 흑색종 간 전이에 대해 가독세틱산 조영증강 자기공명영상을 실시한 67명의 환자들을 대상으로 하였다. 복부영상 전문의 2명이 간 전이의 신호 특성을 형태학적 영상 (조영 전 T1- 및 T2-강조 영상), 확산 강조 영상, 역동적 조영증강 영상 및 간담도기 영상에서 독립적으로 평가하였다. 또한, 간전이의 영상 소견을 간담도기 영상에서의 감지 여부 및 흑색종의 원발 부위에 따라 비교분석 하였다. 여러 자기공명영상 시퀀스 별 간 전이의 진단에 대한 민감도를 일반화 추정 방정식을 사용한 로지스틱 회귀분석을 통해 비교하였다.

2. 포도막 흑색종 간 전이 진단을 위한 가독세틱산 조영증강 자기공명영상의 대안으로서의 비조영 자기공명영상

본 후향적 연구는 포도막 흑색종 간 전이에 대해 가독세틱산 조영증강 자기공명영상을 실시한 27 명의 환자들을 대상으로 하였다. 복부영상 전문의 2명이 간 전이를 진단하기 위해 비조영-자기공명영상 (조영 전 T1- 및 T2- 강조영상 및 확산 강조 영상), 역동적-자기공명영상 (비조영-자기공명영상 및 역동적 조영증강 영상), 전체-자기공명영상 (역동적-자기공명영상 및 간담도기 영상)의 세 가지 자기공명영상 세트를 검토하였다. 전이 진단을 위한 전반적인 진단 성능은 수신자 조작 특성 곡선을 사용하여 평가하였다. 민감도와 양성 예측 값은 일반화 추정 방적식을 사용한 로지스틱 회귀분석을 통해 비교하였다.

결과:

1. 흑색종 간 전이 진단을 위한 가독세틱산 조영증강 자기공명영상의 유용성

총 67명 환자의 254개의 간 전이가 포함되었으며 (여성 44명; 평균 연령 ± 표준 편차, 65.6 ± 13.0세), 간담도기 영상에서는 전이의 76.0% (193/254)가 진단되었으며, 그 중 55.5% (141/254)가 저신호강도를 나타냈다. 간담도기 영상에서 진단되지 않은 대부분의 전이는 포도막 흑색종 (98.4%, 60/61) 기원이었고, 1㎝ 이하였으며 (90.2%,

55/61), T1 고신호강도를 보였다 (98.4%, 60/61). 포도막 이외 흑색종에서 유래된 전이는 포도막 흑색종으로부터의 전이보다 T1 저신호강도, T2 고신호강도, 확산 제한, 동맥기 조영증강 및 간담도기 저신호강도를 더 자주 보였다 ($P \leq 0.019$). 간 전이 진단에 대한 간담도기 영상의 민감도 (76.0%)는 확산강조영상 (65.7%, $P = 0.006$)보다 유의하게 높았지만 형태학적 영상 (98.8%, $P < 0.001$) 및 역동적 조영증강 영상 (97.6%, $P < 0.001$)보다 낮았다.

2. 포도막 흑색종 간 전이 진단을 위한 가독세틱산 조영증강 자기공명영상의 대안으로서의 비조영 자기공명영상

총 27명 환자 중 23명의 환자에서 80개의 간 전이가 진단되었다. 전이를 진단하기 위한 전반적인 진단 성능은 세 가지 자기공명영상 세트 간에 유의한 차이가 없었다 ($P = 0.327$). 수신자 조작 특성 곡선 아래 영역은 비조영-자기공명영상의 경우 0.951(95% CI, 0.911-0.991), 역동적-자기공명영상의 경우 0.967(0.937-0.998), 전체-자기공명영상의 경우 0.963(0.930-0.995)으로, 비조영-자기공명영상과 전체-자기공명영상 간에는 유의한 차이가 없었다. ($P = 0.597$). 그리고 역동적-자기공명영상과 전체-자기공명영상 간에 유의한 차이가 없었다. ($P > 0.999$). 간 전이를 진단하기 위한 민감도는 비조영-자기공명영상의 경우 86.9%(78.1-95.7), 역동적-자기공명영상과 전체-자기공명영상의 경우 모두 91.9%(86.8-97.0)로, 이들 간에 유의한 차이가 없었다 ($P = 0.166$). 양성 예측도는 비조영-자기공명영상의 경우 94.6%(90.0-99.1), 역동적-자기공명영상의 경우 94.8%(90.4-99.2), 전체-자기공명영상의 경우 93.6%(89.1-98.2)로, 이들 간에 유의한 차이가 없었다 ($P = 0.282$).

결론:

간담도기 영상의 흑색종 간 전이 검출에 대한 민감도는 76.0%로, 형태학적 또는 역동적 조영증강영상의 민감도보다 낮았다. 가독세틱산 조영증강 자기공명영상의 간담도기 영상은 흑색종 간 전이를 검출하는 데 거의 이점이 없다고 할 수 있겠다. 비조영-자기공명영상은 전체-가독세틱산 조영증강 자기공명영상과 비교하였을 때 포도막 흑색종 간 전이 진단에 높은 정확도를 보이며, 포도막 흑색종 간 전이를 진단하는 데 있어 가독세틱산 조영증강 자기공명영상의 좋은 대안의 될 수 있겠다.

핵심어: 흑색종; 간; 전이; 자기공명영상; 조영제